ChemComm

COMMUNICATION

View Article Online
View Journal | View Issue

Cite this: *Chem. Commun.*, 2019, **55**, 12348

Received 12th July 2019,
Accepted 16th September 2019

DOI: 10.1039/c9cc05383b

rsc.li/chemcomm

A multimeric MRI contrast agent based on a *closo*-borane scaffold bearing modified AAZTA chelates on the periphery†

Shatadru Chakravarty,[abc] Saurav J. Sarma,[ade] Lalit N. Goswami,[a] Quan-Yu Cai,[af] Erik M. Shapiro,[bc] M. Frederick Hawthorne[a] and Lixin Ma*[af]

A multimeric MRI contrast agent based on the *closo*-borane motif is reported. Twelve copies of a modified AAZTA chelate with an alkyne end group are appended on an azide-functionalized *closo*-borane motif using Cu(I) catalyzed click chemistry. The presence of two water molecules on the Gd-bound AAZTA chelate results in high relaxivity for the closomer *in vitro*/*in vivo*.

Gadolinium based contrast agents (GBCAs) are used in about 40% of all Magnetic Resonance Imaging (MRI) exams.[1] These agents are low-molecular-weight Gd-chelates with a polyamino-polycarboxylato-core, *e.g.*, diethylenetriaminepenta acetic acid (DTPA) or 1,4,7,10-tetraazacyclododecane-1,4,7,10-tetraacetic acid (DOTA).[2] These Gd-chelates must possess high thermodynamic and kinetic stability, coupled with a miniscule metal dissociation rate, in addition to being hydrophilic, and must contain at least one coordinated water molecule available for rapid exchange with bulk water.[3]

MRI for molecular imaging is challenged by the low sensitivity of contrast agents in comparison to other imaging modalities such as Positron Emission Tomography (PET).[4] Indeed, clinical GBCAs have relatively low r_1 relaxivity, a measure of the strength of contrast agent. The key parameters that influence r_1 relaxivity at clinically relevant fields are the hydration number (q), rotational correlation time (τ_R), and the water exchange rate ($1/\tau_M$). To overcome this challenge, GBCAs with optimized parameters (q, τ_R and $1/\tau_M$) need to be designed.[5] One approach to achieve this goal involves the attachment of multiple copies of Gd-chelates to a multimeric scaffold, such as dendrimers, polymers and liposomes, thereby increasing the Gd payload.[6–8] However, the structural complexity of such macromolecules leads to arduous multistep synthesis, complex purification and tedious characterization,[9] although advancements in analytical instrumentation have led to major improvements.[10]

Polyhedral boranes and carboranes are robust molecules with well-established chemistry.[11–14] The icosahedral [*closo*-$B_{12}H_{12}]^{2-}$ (**1**) and its hydroxylated counterpart, [*closo*-$B_{12}(OH)_{12}]^{2-}$ (**2**) provide a functionalized molecular scaffold that can be used to anchor up to twelve radial arms with desired pendant groups even at the generation zero. The B–OH vertices resemble alcohols in their reactivity and consequently 12-fold carboxylate ester, carbamate ether, and 1,2,3-triazole derivatives, described by us as "*closomers*", are now available.[15] Recent advances in the vertex differentiation strategy of the [*closo*-$B_{12}H_{12}]^{2-}$ core provide access to unique closomer motifs with applications in targeted drug delivery and imaging.[16] Compared to dendrimers with similar architecture, closomer derivatives of **2** are smaller in size, possess greater rigidity and a higher degree of symmetry. Further, a more compact representation of peripheral functional groups is presented in closomers as compared to dendrimers with similar 12-fold functionality. Thus, closomers are an exciting potential scaffold for development of multimeric GBCAs with a high payload.

We report herein a new class of monodisperse MRI closomer GBCAs (CCAs) that have twelve radial Gd^{3+}-chelate arms in close proximity, linked to a central rigid *closo*-B_{12} core. The Gd-chelates are based on the 6-amino-6-methylperhydro-1,4-diazepine-1,4-N^6,N^6-tetra acetic acid ring system, better known as AAZTA. Introduced in 2004, the heptadentate AAZTA motif wraps around the central Gd^{3+} ion leaving two inner sphere water molecules (q = 2) in fast exchange with bulk water.[17] Gd-AAZTA exhibits high relaxivity (7.1 s^{-1} mM^{-1} at 20 MHz and 298 K), satisfactory thermodynamic stability and kinetic inertness.[18] The present work builds on recent efforts focusing on the covalent attachment of multiple copies of Gd-chelates on a central core to generate multimeric, medium-size molecules

[a] *International Institute of Nano and Molecular Medicine and Department of Radiology, University of Missouri, Columbia, MO, 65212, USA. E-mail: mal@health.missouri.edu*
[b] *Molecular and Cellular Imaging Laboratory, Department of Radiology, Michigan State University, East Lansing, MI, 48823, USA*
[c] *Institute for Quantitative Health Science and Engineering, Michigan State University, East Lansing, MI, 48823, USA*
[d] *Bond Life Sciences Centre, University of Missouri, Columbia, MO 65201, USA*
[e] *MU Metabolomics Centre, University of Missouri, Columbia, MO, 65201, USA*
[f] *Harry S. Truman Memorial Veterans' Hospital, Columbia, MO 65201, USA*

† Electronic supplementary information (ESI) available: Physicochemical characterization of all compounds, *in vitro* and *in vivo* MRI studies for Gd-chelates and closomer-Gd-AAZTA complexes. See DOI: 10.1039/c9cc05383b

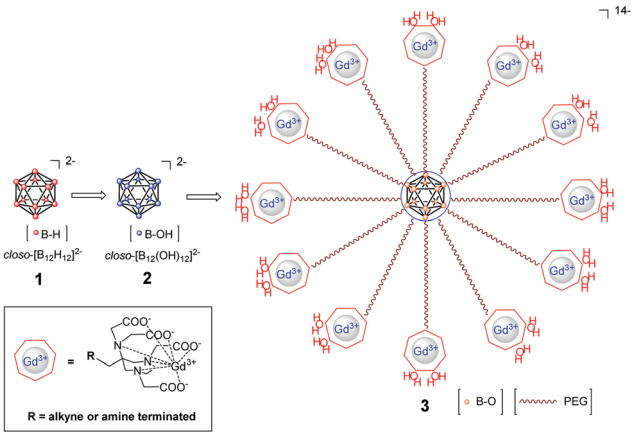

Fig. 1 Icosahedral *closo*-borane scaffold decorated with twelve Gd-AAZTA chelate arms. The linker arms consist of PEG chains and are linked with the *closo*-borane cage using either a triazole or a carbamate linkage.

as GBCAs for MRI.[15] Our general approach is represented in Fig. 1, with **3** being the target CCA. The peripheral AAZTA ligands are modified using amine/alkyne terminated PEG linkers for conjugation with the closomer core. The resulting configuration yields a multifunctional molecule with a symmetric, compact and globular architecture with high molecular relaxivity. This chemistry can be extended to various targets/chelates for biomedical applications.

Our initial goal involved the synthesis of novel amine- and alkyne- terminated AAZTA analogues, AAZTA-NH_2 and AAZTA-alkyne, respectively that could then be appended on the closomer using well established chemistry.[15] The synthesis of AAZTA-NH_2, **12** is detailed in Scheme 1. The first step involves the nucleophilic substitution of the pendant halogen in commercially available 2-(2-(2-chloroethoxy)ethoxy) ethanol, **4** using NaI in acetonitrile (ACN), followed by $AgNO_2$ assisted nucleophilic substitution of the iodo group in **5** with a nitro functionality to afford **6**. Next, a double nitro Mannich reaction between *N*,*N*′-dibenzyl ethylenediamine, paraformaldehyde and **6**, generates the 1,4-nitro diazepine ring, **7**. This was the key step to generate the seven-membered diazepine ring akin to the AAZTA ligand. This reaction was straightforward and was successfully scaled up to 20 g, with very good yield. The purification of the crude reaction mixture was straightforward on grade IV alumina and the desired product, **7** was obtained in 86% yield as a colorless viscous oil. Next, a one pot reduction of the pendant nitro and the *N*-benzyl groups *via* catalytic hydrogenation affords highly basic triamine **8**. Exhaustive alkylation of **8** using a 5-fold excess of *tert*-butyl bromoacetate yields the substituted AAZTA-OH tetra-ester **9** in 68% yield. The terminal hydroxyl group in **9** was replaced with a bromide to yield AAZTA-Br, **10** in 92% yield. The next step involved substitution of the pendant bromide with a phthalimide group to obtain **11**, followed by hydrazine assisted reduction to yield the desired AAZTA-NH_2, **12** as a colorless viscous oil in over 90% yield. All the steps in the sequence result in good to excellent yields and purification of the intermediates was simple and straightforward.

To demonstrate the reactivity of the peripheral –NH_2 and –OH functionalities and subsequently introduce an alkyne end group, **12** was fused with 5-hexynoic acid *via* EDC/DMAP assisted coupling to afford **13** in quantitative yields (Scheme 2). Similarly, a short PEG chain linker, **14** (Scheme S1, ESI†) carrying orthogonal alkyne and amine end groups was conjugated with **9** using 1,1′-carbonyldiimidazole (CDI) assisted coupling to afford **15** in excellent yields (Scheme 2).

The generation of various AAZTA analogues with induced disparities in the nature and length of the linker arm allows us to investigate their influence on the relaxivity of the final Gd-chelates. Thus, the precursor esters **9**, **12**, **13** and **15** were subjected to a two-step procedure to formulate the corresponding Gd-chelates (Scheme S2, ESI†) in excellent yield. The first step involved the removal of the pendant *tert*-butyl ester groups using 95% formic acid to yield the tetra-acid ligands (**L1–L4**), followed by Gd-complexation of the crude product using $GdCl_3{\cdot}6H_2O$ to obtain the desired product (**Gd-L1–Gd-L4**). The synthesis and purification of the Gd-chelates is detailed in the ESI.† The r_1 relaxivity for all the Gd-chelates, analyzed in PBS (pH 7.4) and bovine calf serum, ranged within 7 to 8 s^{-1} mM^{-1} (Table S1, ESI†), which is in agreement with various Gd-AAZTA chelates reported to date. Further, their relaxivity is also two-fold higher than clinically used Gd-DOTA or Gd-DTPA chelate. The higher relaxivity can be linked to their q = 2 value as compared to the q = 1 for Omniscan. The q value was calculated by measuring the Dy^{3+}-induced water ^{17}O NMR shift for the corresponding Dy(III) complex Dy-L3 (Scheme S3, eqn (S1)–(S3), Fig. S1 and Table S2, ESI†).[19] A greater q value ensures enhanced interaction of the bound water with the metal electron spins; and consequently amplified values for r_1 are obtained. Further, the subtle structural modifications within the side arm does not interfere with the

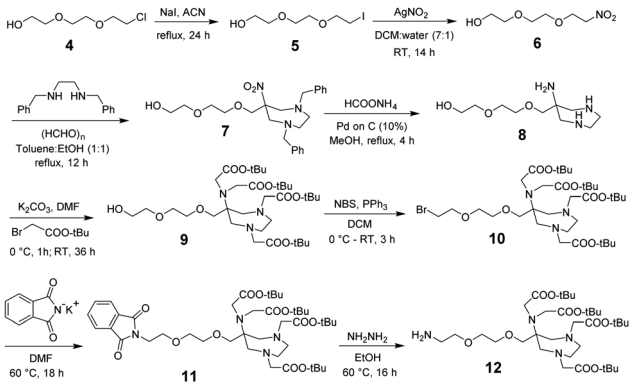

Scheme 1 Synthesis of amine terminated AAZTA analogue.

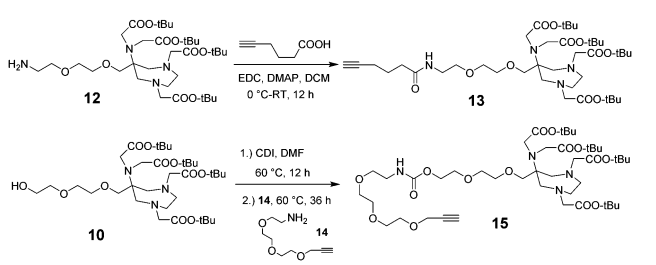

Scheme 2 Synthesis of alkyne terminated AAZTA analogues.

donor (ligand)–acceptor (metal core) interaction and therefore the relaxivity of the final Gd-chelate remains unaltered.

Having streamlined the synthesis of amine- and alkyne terminated AAZTA analogues, conjugation with the closomer core was next pursued. For 12-fold conjugation, both linker types have been previously employed, utilizing available carbonate- and azide-functionalized closomer derivatives. As a proof of concept, **11** with an amine end group, was readily conjugated with the 12-fold carbonate closomer, **C1** using ACN as the solvent and an excess of DIPEA as the base at ambient conditions for 7 days to afford the corresponding 12-fold AAZTA carbamate closomer, **C2** (Scheme S4, ESI†).

Next, conjugation of the alkyne-terminated AAZTA, **13** with the closomer was investigated. For quantitative 12-fold functionalization of the closomer scaffold, Cu(I) catalyzed 1,3-dipolar cycloaddition with the dodeca(azidoester) closomer, **C3** was pursued (Scheme 3). **C3** was initially synthesized using a reported procedure.[20] Next, it was reacted with 60-fold excess of **13** over 4 days to afford the desired AAZTA-triazole closomer **C4** in 75% yield. To enhance the solubility of the reagents employed in the reaction, a 1 : 1 mixture of solvents THF and ACN were used. For optimal reaction yields, **13** and **C3** were mixed and dried thoroughly under high vacuum. CuI, DIPEA and the requisite solvents were next added in rapid succession and the mixture was stirred at RT for 4 days. Reaction progress was monitored using periodic ^{11}B NMR analysis of the crude reaction mixture and was ascertained complete on appearance of a sharp singlet in the ^{11}B NMR spectra, centered around −18 ppm. Further proof of complete 12-fold functionalization was evident from the disappearance of the characteristic IR peak for the azide group at 2100 cm^{-1}, and consequent appearance of a characteristic singlet at δ 7.07 ppm in the ^{1}H NMR spectrum, assigned to the alkene-CH protons of the twelve triazole rings (ESI†). Purification of the crude reaction mixture using Size Exclusion Chromatography (SEC, LH-20 Sephadex) yielded pure **C4** as a brown colored very viscous oil. It was extensively characterized using NMR, IR and HRMS. **C2** and **C4** present the first of their kind closomer derivatives appended with twelve copies of a modified AAZTA linker.

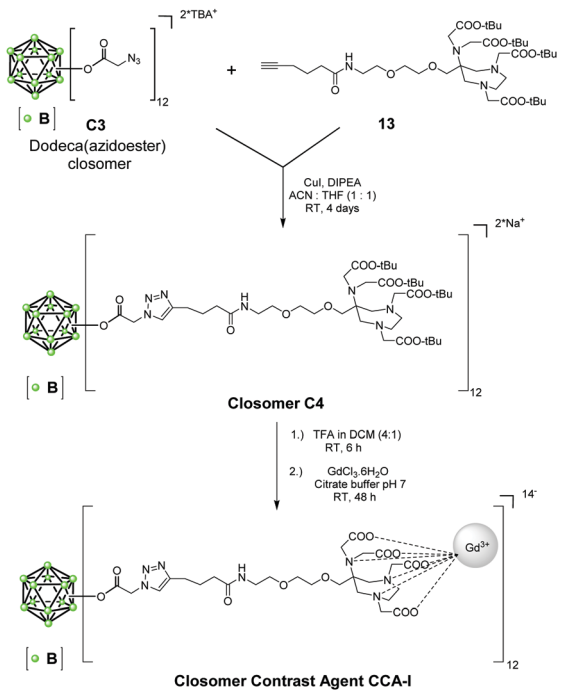

Scheme 3 Synthesis of the Closomer Contrast Agent, **CCA-I**.

Generation of the final closomer contrast agent, **CCA-I** was straightforward. The pendant *tert*-butyl ester groups were first removed using 80% trifluoroacetic acid in DCM (Scheme 3); complete de-protection was confirmed by the disappearance of the prominent singlet at δ 1.42 ppm in the ^{1}H NMR spectrum attributed to *tert*-butyl groups (Fig. S2, ESI†). A sharp singlet in the ^{11}B NMR spectra indicated that 12-fold integrity was maintained at the closomer cage (Fig. S3, ESI†). Subsequently, the product was reacted with $GdCl_3{\cdot}6H_2O$ in citrate buffer at pH 7 to obtain **CCA-I** in 79% yield. **CCA-I** was purified *via* exhaustive dialysis against ultrapure water and the product was characterized using IR and inductively coupled plasma optical emission spectroscopy (ICP-OES). The IR spectrum displayed a shift for the C=O stretch from 1736 cm^{-1} to 1607 cm^{-1} demonstrating the complexation of Gd^{3+} with carboxylate oxygen in AAZTA (Fig. S4, ESI†). The Gd loading was determined using ICP-OES, which showed an average of 10.8 Gd^{3+} ions per closomer unit in **CCA-I**.

CCA-I displayed high r_1 value of 9.1–9.3 s^{-1} mM^{-1} per Gd (98.3–100.4 s^{-1} mM^{-1} per closomer) at 25 °C and 7 T in PBS and serum. The more than 220% increase in the r_1 value for **CCA-I** over Omniscan and Dotarem (r_1 = 4.05 s^{-1} mM^{-1} and 3.6 s^{-1} mM^{-1}, respectively at 7 T) can be largely attributed to q = 2 for individual chelates, with additional enhancement from the confinement of the twelve Gd^{3+}-AAZTA chelates in a sterically constrained space. Such close packing further restricts internal rotation of the chelates and consequently increases the per-Gd relaxivity of **CCA-I** as compared to that of individual Gd-AAZTA chelate, **Gd-L3** (r_1 = 7.3 s^{-1} mM^{-1}; Fig. S5, ESI†). The increase in r_1 for **CCA-I** is however, lower than the 300% enhancement reported for a similar multimeric CCA carrying heptadentate DTTA chelates around the B_{12}-core.[21] This could be attributed to a short and compact linker arm used for conjugating the DTTA ligand to the B12-core, thereby lowering the internal rotation of the linker arms, resulting in higher overall relaxivity. Traditionally, Gd-AAZTA chelates demonstrate higher kinetic stability and resistance to transmetallation with endogenous ions as compared to Gd-DTTA,[22] thus making them attractive for clinical translation.[23] Dynamic light scattering (DLS) analysis of **CCA-I** in both PBS and serum measured average particle size of 900 nm, indicating possible aggregation. To negate the possibility of a high r_1 value due to aggregation, a formulation of **CCA-I** in 2% TWEEN-80 was prepared that lowered its average particle size to 20 nm (Fig. S6, ESI†). The relaxivity measurements of this formulation at 7 T gave an r_1 value of 9.4 s^{-1} mM^{-1}, almost identical to that obtained in PBS (Fig. 2A). Table S3 in ESI† summarizes the relaxivity profiles of some of the poly-functional MRI CAs reported to date, and **CCA-I** compares very favorably. Fig. 2B shows the T_1-weighted MRI of **CCA-I** compared to Omniscan at different Gd concentrations (0, 0.1, 0.5 and 1 mM) in PBS, clearly endorsing the greater contrast enhancement of **CCA-I** than Omniscan.

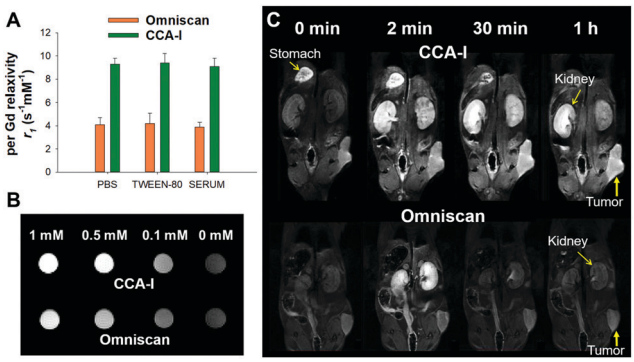

Fig. 2 (A) Comparison of per Gd r_1 relaxivity for **CCA-I** and Omniscan in PBS, 2% TWEEN-80 and bovine calf serum at 7 T and 25 °C. (B) T_1-Weighted MRI of **CCA-I** at various concentrations in PBS compared with Omniscan. (C) *In vivo* T_1-weighted MRI of SCID mice bearing PC-3 tumors before, 2 min, 30 min and 1 h after intravenous injection of **CCA-I** (top) and Omniscan (bottom) at a Gd dose of 0.04 mmol kg^{-1} and 7 T.

Finally, the *in vivo* potential of **CCA-I** was investigated in severely compromised immunodeficient (SCID) mice bearing human PC-3 prostate cancer xenografts. Six mice per group were given intravenous injections of **CCA-I** or Omniscan at a Gd dose of 0.04 mmol kg^{-1} body weight. Sequential T_1-weighted MRI was performed pre and post-injection. The **CCA-I** group exhibited strong and prolonged tissue enhancement in tumor and kidneys compared to the Omniscan group (Fig. 2C). Tumor signal enhancement by **CCA-I** persisted up to 4 h followed by complete renal clearance in 24 h (Fig. S7, ESI†). Quantitative analysis showed that the contrast enhancement ratio (CER) by **CCA-I** was significantly higher in tumors at 30 min and 1 h and in kidneys at 1 h than that by Omniscan (Fig. S8, ESI†).

In summary, we hereby report a monodisperse, nano-sized, multimeric closomer MRI contrast agent **CCA-I**, based on icosahedral *closo*-borane scaffold. The unique configuration of twelve modified Gd-AAZTA chelates configured tightly in a sterically confined space exhibits high relaxivity. New versions of the AAZTA chelate, with functionalizable amine, hydroxyl and alkyne end groups are also reported that can be used as precursors for attachment to various biological targets.

This research was funded by National Cancer Institute (R21-CA114090) and University of Missouri, MO 65212, USA. E. M. S. was funded by National Institute of Diabetes and Digestive and Kidney Diseases (R01-DK-107697). L. M. was funded by Department of Defense Prostate Cancer Research Program (DoD W81XWH0920176). Authors thank Brett Meers for technical assistance, and facility support of Truman VA Biomolecular Imaging Center, MO 65201, USA.

Conflicts of interest

There are no conflicts to declare.

Notes and references

1 V. M. Runge, *Invest. Radiol.*, 2017, **52**, 317–323.
2 J. Wahsner, E. M. Gale, A. Rodríguez-Rodríguez and P. Caravan, *Chem. Rev.*, 2019, **119**, 957–1057.
3 S. Aime, D. D. Castelli, S. G. Crich, E. Gianolio and E. Terreno, *Acc. Chem. Res.*, 2009, **42**, 822–831.
4 M. A. Pysz, S. S. Gambhir and J. K. Willmann, *Clin. Radiol.*, 2010, **65**, 500–516.
5 T. J. Clough, L. Jiang, K.-L. Wong and N. J. Long, *Nat. Commun.*, 2019, **10**, 1420.
6 H.-K. Kim, G. H. Lee and Y. Chang, *Future Med. Chem.*, 2018, **10**, 639–661.
7 S. M. Vithanarachchi and M. J. Allen, *Curr. Mol. Imaging*, 2012, **1**, 12–25.
8 J. L. Major and T. J. Meade, *Acc. Chem. Res.*, 2009, **42**, 893–903.
9 I. Craciun, G. Gunkel-Grabole, A. Belluati, C. G. Palivan and W. Meier, *Nanomedicine*, 2017, **12**, 811–817.
10 J. R. Lloyd, P. S. Jayasekara and K. A. Jacobson, *Anal. Methods*, 2016, **8**, 263–269.
11 S. P. Fisher, A. W. Tomich, S. O. Lovera, J. F. Kleinsasser, J. Guo, M. J. Asay, H. M. Nelson and V. Lavallo, *Chem. Rev.*, 2019, **119**, 8262–8290.
12 S. P. Fisher, A. W. Tomich, J. Guo and V. Lavallo, *Chem. Commun.*, 2019, **55**, 1684–1701.
13 J. C. Axtell, L. M. A. Saleh, E. A. Qian, A. I. Wixtrom and A. M. Spokoyny, *Inorg. Chem.*, 2018, **57**, 2333–2350.
14 R. Núñez, M. Tarrés, A. Ferrer-Ugalde, F. F. de Biani and F. Teixidor, *Chem. Rev.*, 2016, **116**, 14307–14378.
15 M. F. Hawthorne and A. Pushechnikov, *Pure Appl. Chem.*, 2012, **84**, 2279.
16 S. J. Sarma, A. A. Khan, L. N. Goswami, S. S. Jalisatgi and M. F. Hawthorne, *Chem. – Eur. J.*, 2016, **22**, 12715–12723.
17 S. Aime, L. Calabi, C. Cavallotti, E. Gianolio, G. B. Giovenzana, P. Losi, A. Maiocchi, G. Palmisano and M. Sisti, *Inorg. Chem.*, 2004, **43**, 7588–7590.
18 Z. Baranyai, F. Uggeri, G. B. Giovenzana, A. Bényei, E. Brücher and S. Aime, *Chem. – Eur. J.*, 2009, **15**, 1696–1705.
19 M. C. Alpoim, A. M. Urbano, C. F. G. C. Geraldes and J. A. Peters, *J. Chem. Soc., Dalton Trans.*, 1992, 463–467.
20 L. N. Goswami, S. Chakravarty, M. W. Lee, S. S. Jalisatgi and M. F. Hawthorne, *Angew. Chem., Int. Ed.*, 2011, **50**, 4689–4691.
21 L. N. Goswami, L. Ma, S. Chakravarty, Q. Cai, S. S. Jalisatgi and M. F. Hawthorne, *Inorg. Chem.*, 2013, **52**, 1694–1700.
22 E. Brücher, G. Tircsó, Z. Baranyai, Z. Kovács and A. D. Sherry, *The Chemistry of Contrast Agents in Medical Magnetic Resonance Imaging*, John Wiley & Sons, Ltd, Chichester, UK, 2013, pp. 157–208.
23 Bracco S.p.A., *Eur. Pat.*, EP1964846 (A1), Universita di Trieste, Italy, 2008, p. 34; Chemical Indexing Equivalent to 149:326295.